ELSEVIER

Journal of Structural Geology 28 (2006) 2259–2269

JOURNAL OF STRUCTURAL GEOLOGY

www.elsevier.com/locate/jsg

Folding of Europa's icy lithosphere: an analysis of viscous-plastic buckling and subsequent topographic relaxation

Andrew J. Dombard [a,b,*], William B. McKinnon [a]

[a] *Department of Earth and Planetary Sciences and the McDonnell Center for Space Sciences, Washington University, Saint Louis, MO 63130*
[b] *Planetary Exploration Group, Space Department, The Johns Hopkins University Applied Physics Laboratory, Laurel, MD 20723, USA*

Received 12 April 2005; received in revised form 30 November 2005; accepted 6 December 2005
Available online 24 January 2006

Abstract

Potential contractional folds on Jupiter's icy moon Europa have been identified. The best example is at the extensional band Astypalaea Linea, where a series of subtle topographic undulations, 25 km in wavelength, possess parasitic tectonic features that support a folding origin. A scenario has been qualitatively proposed, whereby folds form via unstable contraction of the icy lithosphere, compensate for extension elsewhere on Europa, and then subsequently relax. Here, we quantitatively address this scenario, applying a model for viscous-plastic buckling of planetary lithospheres and finite element simulations of topographic relaxation. Our results suggest that the lithosphere of Europa could indeed be unstable, but the low required surface temperatures limit fold formation to higher latitudes, and the high required driving stresses (~9–10 MPa) are difficult to achieve on the satellite. The depth to the brittle–ductile transition is well constrained, and high thermal gradients are indicated, implying heat flows near 100 mW m^{-2}. In addition, topographic relaxation progresses so slowly even at these heat flows that it is not a viable mechanism to eliminate such features over the age of Europa's surface. Given the paucity of identified folds, we conclude that the necessary conditions for their formation are rare and that lithospheric folding is a minor mechanism for compensating the large amounts of extension seen elsewhere on Europa.

Keywords: Jovian satellites; Europa; tectonics; Folding

1. Introduction

The surface of Jupiter's icy moon Europa presents an intriguing puzzle. Evidence from geophysical measurements and spectroscopy indicate a largely rocky world, 1565 km in radius, whose outer ~100–150 km is mostly H_2O (for a recent review, see Greeley et al. (2004)). This H_2O layer is further subdivided in to a liquid water layer overlain by an ice shell ~10–30 km thick (Pappalardo et al., 1999; Schenk, 2002). While the surface geology of Europa displays ample evidence for tectonism, the vast majority of such features are extensional or strike-slip in nature. Ridges, troughs, and pull-apart bands are ubiquitous and record large amounts of extension of the icy shell. Despite all this extension and other motion, however, few candidate examples of tectonic features contractional in nature that can compensate the extension have been identified (Prockter and Pappalardo, 2000; Sarid et al., 2002).

Prockter and Pappalardo (2000) identified a series of ~3 subtle, periodic undulations of the surface near Astypalaea Linea (~69° S, 198° W), a topographically relatively smooth band at high southern latitudes on Europa (Fig. 1). These undulations have a wavelength of ~25 km and stereo-determined crest-to-trough elevation differences of ~250±50 m (P.M. Schenk, personal communication, 2005). The interpretation that these undulations represent folds in Europa's lithosphere is supported by the identification of linear tectonic features following the strike of the folds and occurring in the troughs and on the crests. On the crest tops, where zones

* Corresponding author. Fax: +240 228 8939.
E-mail address: andrew.dombard@jhuapl.edu (A.J. Dombard).

0191-8141/$ - see front matter © 2005 Elsevier Ltd. All rights reserved.
doi:10.1016/j.jsg.2005.12.003

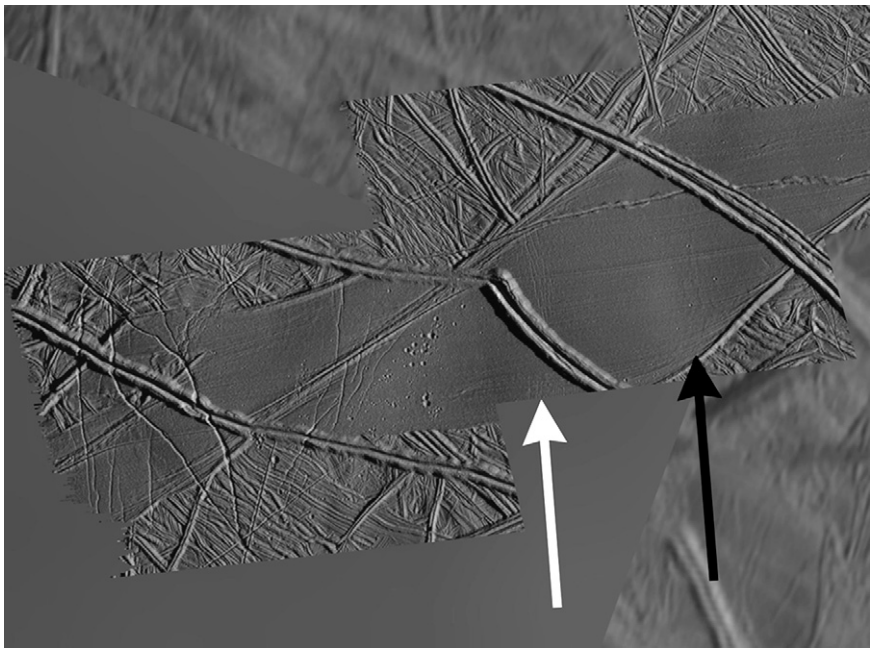

Fig. 1. A view of Astypalaea Linea, composed of Galileo images superposed over regional Voyager coverage. Subtle shading variations and smaller scale, complementary tectonic structures suggest a possible lithospheric fold. A crest of the fold is highlighted by the white arrow, a trough with a black arrow; the spacing of the arrows is ~12.5 km. (Image kindly supplied by P.M. Schenk.)

of tension in a folding layer might be expected, small-scale fractures are observed, whereas in the trough bottoms (zones of compression), sub-parallel, small-scale ridges are observed and are inferred to be contractional structures.

A small number of other potential folds have been identified on Europa (Figueredo and Greeley, 2000; Prockter and Pappalardo, 2000; Prockter et al., 2002), but the case for folding is less compelling than that at Astypalaea Linea. The Astypalaea Linea region provides a relatively featureless region within which the folds and associated structures can be identified, and was favorably imaged at relatively low sun (13° from horizontal). The other potential folds are, in some cases, single swells or crests, or found on topographically rough terrain, and thus may be due to other causes. Large amplitude (~1 km), arcuate parallel depressions do exist on Europa (Schenk, 2005), but they are of much larger wavelength, probably are extensional in origin, and thus are unrelated to the style of deformation seen at Astypalaea Linea.

Based on the identification of these folds, Prockter and Pappalardo (2000) suggested an evolutionary scenario by which folds form and are destroyed on Europa. They proposed that compressional stresses under conditions of high heat flow resulted in the generation of a lithospheric instability (i.e. folding), compensating extension elsewhere on the satellite. Subsequently, these folds relaxed away geologically quickly, implying that even more contractional strain may have been taken up. These authors supported this proposed scenario with preliminary calculations. Here, we address the formation and destruction of folds on Europa more quantitatively, finding that while it is possible for the lithosphere to fold, the conditions are likely rare, and that topographic relaxation of these features is inefficient. Europa likely compensates its pervasive surface extension in some other way.

2. Lithospheric folding

2.1. Model

We use the well-known model for unstable deformation of the lithosphere of Fletcher and Hallet (1983). Originally developed for plane-strain extension (i.e. development of 'plastic' necking instabilities) in the Basin and Range Province of the western United States, this model was applied in a preliminary form to the creation of the extensional grooved terrain (undulations with a dominant wavelength of order 10 km) on Ganymede, Jupiter's largest moon (Fink and Fletcher, 1981) and subsequently has been applied to the compressional deformation of the Central Indian Basin (Zuber, 1987) and again to the formation of Ganymede's grooved terrain (Herrick and Stevenson, 1990; Dombard and McKinnon, 2001). We follow the treatment in Dombard and McKinnon (2001).

2.1.1. Basics

In this derivation, the Navier–Stokes equations are solved for planar, perturbing flow superposed on uniform, horizontal flow in a compositional half-space. Mechanically, the half-space consists of a viscous substrate underlying a lithosphere assumed to be pervasively fractured on a sufficiently small length scale so as to behave plastically. We do not specifically model Europa's underlying liquid water ocean because relative to the strength of the lithosphere, the warm (weak) deep ice and liquid water are essentially inviscid and negligibly

distinguishable; consequently, this model cannot be used to address the total thickness of the ice shell (a critically important problem in Europa science), other than it must be thicker than our modeled lithosphere and viscous substrate combined. A linear, time-independent thermal structure is also assumed. Solutions are found for a range of wavelengths, with the fastest growing one defining the dominant solution and thus the wavelength of the most amplified topography that is ultimately observed. The original derivation (Fletcher and Hallet, 1983) was for extension (i.e. necking instabilities); however, the conversion to contraction (folding or viscous-plastic buckling) is straightforward.

2.1.2. Rheology

The constitutive relation for both layers follows a power law, where the equivalent strain rate is proportional to the equivalent deviatoric stress raised to a power n. In a power-law material as n asymptotically approaches infinity, an increment of stress produces a near infinite rate of deformation, essentially resulting in plasticity (i.e. time-independent, permanent deformation, where the material responds instantly to an applied stress increment). For this paper, we set the value of n in the surface plastic layer to 10^6 (see Dombard and McKinnon, 2001). We set the thickness of the plastic layer as the depth to the brittle–ductile transition (BDT), which is determined via the standard method using a yield strength envelope (Brace and Kohlstedt, 1980) (Fig. 2). This surface layer is then assumed to possess a strength (i.e. viscosity) constant with depth and equal to the value at this interface (the BDT), whereas the viscosity of the substrate is approximated as decaying exponentially with depth (the e-folding depth determined by evaluating the depth-derivative of the ductile flow law at the interface). There exists some debate over the best way to relate the modeled plastic lithosphere and viscous substrate to the yield strength envelope (e.g. Fletcher and Hallet, 2004); however, setting the thickness of the plastic layer to the depth to the BDT maximizes instability strength.

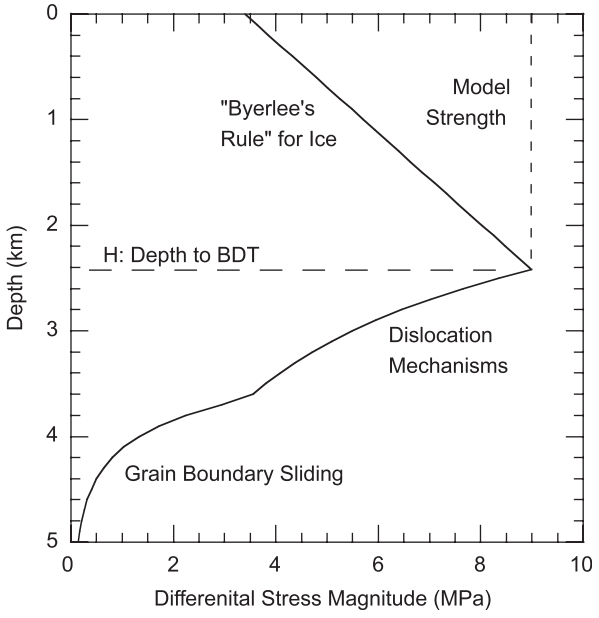

Fig. 2. An example of a yield strength envelope in compression on Europa, assuming a surface temperature of 80 K, a thermal gradient of 18 K km^{-1}, and a shortening rate of 10^{-15} s^{-1}. The brittle portion is defined by a frictional slip criterion with finite cohesion (Beeman et al., 1988), while the ductile portion is controlled by a host of creep mechanisms (Durham and Stern, 2001; Goldsby and Kohlstedt, 2001). At these conditions, the depth to the brittle/ductile transition (BDT) H is ~2.4 km. Creep below this depth is controlled by dislocation mechanisms, with a transition at greater depth to a mechanism inferred to be grain boundary sliding (assuming a 1 mm grain size). The depth-independent strength used in the instability model is indicated.

A yield strength envelope must be evaluated in order to determine the characteristics of our modeled viscous-plastic system. For the brittle portion of the yield strength envelope, we use the frictional law determined by Beeman et al. (1988), effectively a 'Byerlee's rule' for cold ice. At low confining pressures, these experiments allowed two relationships between failure shear stress (τ) and normal stress (σ_n) consistent with the data, one with finite cohesion and one with zero cohesion:

$$\tau = 0.55\sigma_n + 1.0\ \text{MPa} \tag{1a}$$

$$\tau = 0.69\sigma_n \tag{1b}$$

To be thorough, we implement both fits. In plane-strain compression, the failure criterion with a cohesion of 1 MPa (Eq. (1a)) converts to a zero-pressure yield strength of 3.4 MPa (see Beeman et al., 1988).

For the viscous portion of the yield strength envelope, there are several creep mechanisms in ice that can dominate its flow under different thermal and stress states (Durham and Stern, 2001; Goldsby and Kohlstedt, 2001; see also Table I in Dombard and McKinnon, 2001). We employ a trio of grain-size insensitive, dislocation creep mechanisms (Durham and Stern, 2001). These flow laws are denoted A, B, and C, with the transition between the three a function of decreasing temperature (although ductile A does not end up being important). These creep mechanisms operate in series (i.e. the fastest one dominates the flow) along with a pair of additional creep mechanisms that operate in a rate-limiting sense (Goldsby and Kohlstedt, 2001); these latter flow laws describe creep along an easy-slip system (ES) and a grain-size-sensitive deformation mechanism, argued by Goldsby and Kohlstedt (2001) to be grain boundary sliding (GBS). This last mechanism introduces ice grain size as an additional model parameter. Taking glacial ice as a plausible terrestrial analogue, we assume a grain size range of 0.1–10 mm (Souchez and Lorrain, 1991; De La Chappelle et al., 1998; Dombard and McKinnon, 2001).

Because there are multiple creep mechanisms that may be operating, the viscosity structure of the substrate may only be piece-wise continuous (see Fig. 2), a situation not accounted for in the original derivation of Fletcher and Hallet (1983). Dombard and McKinnon (2001) used an averaging scheme to determine an effective power-law exponent and e-folding depth for the substrate viscosity structure, a scheme adopted here.

2.1.3. Dimensionless growth rate

This treatment is based on a perturbation analysis, whereby the perturbing flow is independently solved for each Fourier component of topography. The time rate of change of the amplitude of these components $h(\lambda)$ is given by

$$\frac{\partial h\left(\lambda\right)}{\partial t} = w\left(\lambda\right) + \left|\bar{D}_{xx}\right| h\left(\lambda\right) \tag{2}$$

where λ is wavelength, $w(\lambda)$ is the Fourier component of the vertical perturbing velocity at the surface, and the second term on the right-hand side, the product of the absolute value of the background rate of shortening deformation and the currently topographic amplitude, accounts for the passive amplification of pre-existing topography due to uniform contraction. The dimensionless growth rate is defined as the ratio of the vertical velocity of the perturbing flow to the growth due to passive amplification:

$$q = \frac{w\left(\lambda\right)}{\left|\bar{D}_{xx}\right| h\left(\lambda\right)} \tag{3}$$

There is a range of possible q, corresponding to the continuum of the Fourier wavelength spectrum. The maximum value $q_{\max}$ corresponds to the fastest growing Fourier component of topography and hence the observed fold. With this concept and Eqs. (2) and (3), the amplitude of the observed fold $h_{\max}$ is

$$\ln\left(\frac{h_{\max}}{h_{\mathrm{o}}}\right) = \left(q_{\max} + 1\right)\left(\left|\bar{D}_{xx}\right| t\right) \tag{4}$$

where h_{o} is the initial amplitude and $\left|\bar{D}_{xx}\right| t$ is total amount of horizontal shortening (assumed to be small; see below).

The critical growth rate needed to yield the folds observed near Astypalaea Linea can be estimated. As noted above, the crest-to-trough elevation difference of the folds is ~250 m (fold amplitudes h of ~125 m). Assuming that the amplitude of initial topographic 'white noise' was several meters, a total amplification factor of ~25–40 is indicated, which is also the approximate amplification factor needed for the fastest growing spectral component to become observably dominant in three-dimensional folding simulations of a power-law layer embedded in a viscous medium (Fletcher, 1995). Prockter and Pappalardo (2000) estimated the range of horizontal shortening compensated by the folds as $\pi^2 h^2/\lambda^2$ for sinusoidal folds that conserve length (parallel folding). For h=125 m and λ=25 km, the shortening is ~0.025%, a very small number. Unfortunately, a viscously or plastically failing lithosphere does not conserve surface length, and there is no way to reliably estimate the horizontal strain from the shape of the folds alone (the estimate above is a lower bound). Numerical models of folding indicate that the vertical strain is a better but still imprecise guide (the relationship between vertical and horizontal strain depends on, among other things, the precise viscosity structure modeled; Zuber and Parmentier, 1996). The vertical strain at Astypalaea Linea is ~2%. This value represents a very coarse estimate of the horizontal strain, and the actual horizontal strain in this region is likely different. If we apply this value to Eq. (4), we find that $q_{\max}$ must exceed ~160–185. To be conservative, we adopt a minimum growth rate of 200 in order to explain the folds at Astypalaea, but recognize that $q_{\max}$ may be different.

2.1.4. Other parameters

A gravitational acceleration of 1.31 m s^{-2} and a cold, nonporous, ice density of 950 kg m^{-3} are used; the results are not sensitive to modest variations in these values. Additionally, we assume surface temperatures of 80 and 110 K, the former appropriate to mid- to high-latitudes (e.g. Astypalaea Linea) and the latter appropriate to equatorial regions on Europa (Ojakangas and Stevenson, 1989, Appendix A).

A broad range in possible horizontal shortening rates, 10^{-19}–10^{-12} s^{-1}, is considered. A strain rate of 10^{-14} s^{-1} is considered typical for orogenic processes on Earth (e.g. Pffifner and Ramsay, 1982) and corresponds to the build-up of 1% strain over 3×10^4 yr. This time scale is similar to the lower limit of non-synchronous rotation of Europa determined by comparing Voyager and Galileo imagery, 12 kyr (Hoppa et al., 1999), which is a plausible stress source for Europa that we will discuss below. In detail, non-synchronous stresses build up over a quarter cycle of rotation (3 kyr at minimum), so 1% strain in this time period requires a shortening rate of 10^{-13} s^{-1}. In contrast, theoretical considerations place the non-synchronous rotation period at ~10 Myr (Ojakangas and Stevenson, 1989), depending on shell thickness, suggesting the possible build-up of 1% shortening at rates as low as of ~10^{-16} s^{-1}. The age of Europa's surface is itself geologically young and constrained by impact crater counts and models of the cometary impact flux to be ~60 Myr (Zahnle et al., 2003; Schenk et al., 2004). Astypalaea Linea (the band) is relatively young in a Europan context but cut by several ridges and cracks. Hence, it probably formed in the last half to third of Europa's recorded surface history. If the folds do only record very minor amounts of horizontal shortening (say, ~0.1%) over this time scale, then (strain) shortening rates as low as ~10^{-18} s^{-1} (or lower) are in principle possible, but we consider such slow rates implausible.

2.2. Results

Fig. 3 plots contours of the dominant growth rate $q_{\max}$ and the 25-km-wavelength contour, as a function of thermal gradient and horizontal shortening rate. In addition, we identify the creep mechanisms that are averaged to define the substrate viscosity structure. A first-order observation is that growth rates are generally high across a broad range of grain sizes and thermal gradients, and for either rule for the frictional strength of ice (Beeman et al., 1988). This is a consequence of the low temperature of high-latitude surfaces on Europa (see Dombard and McKinnon, 2001) and helps explain the existence of folding on Europa, at least at higher latitudes.

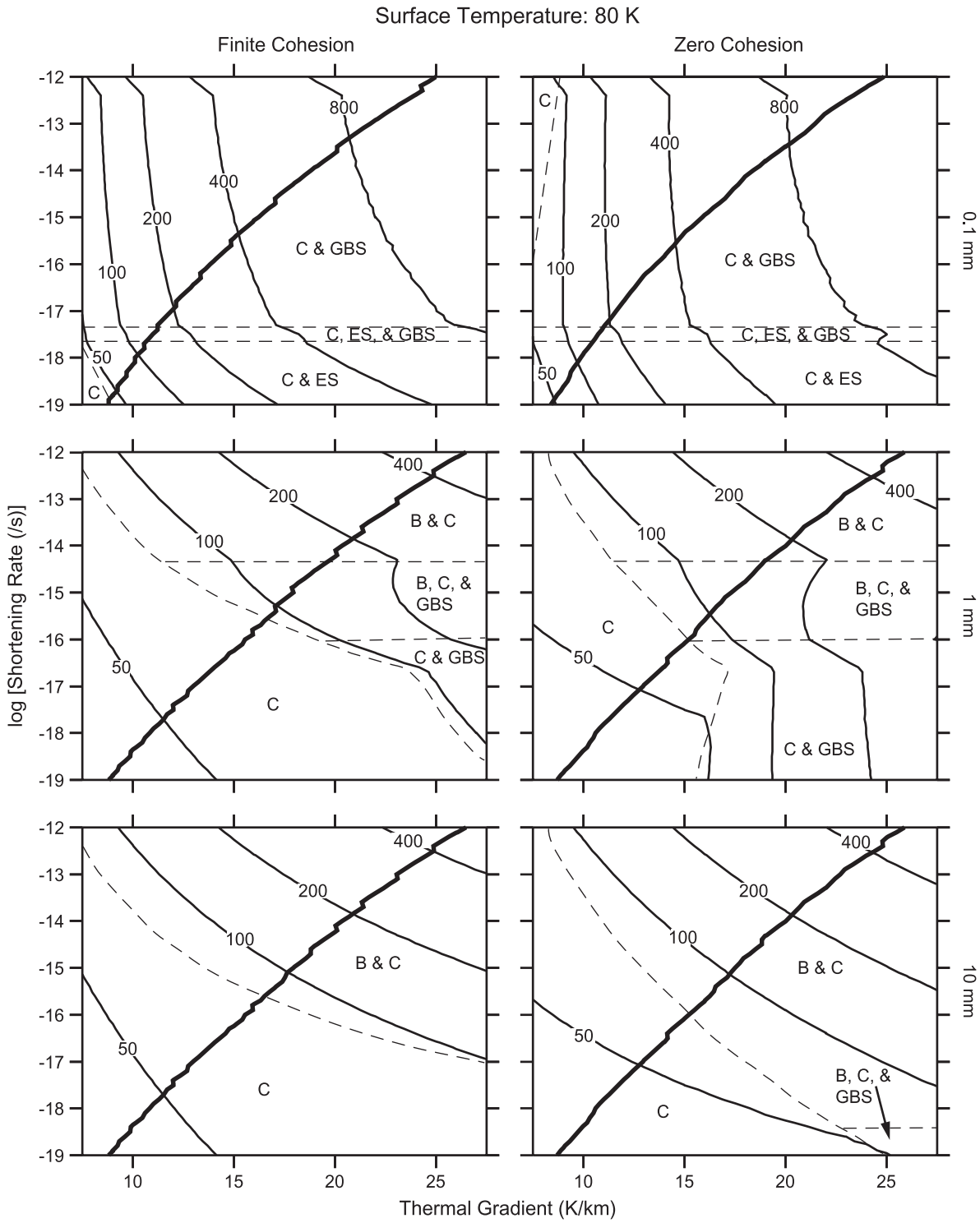

Fig. 3. Contours of the dominant dimensionless growth rate q_{max} (thin solid lines) and a contour of the 25 km wavelength (thick solid line) as a function of horizontal shortening rate and thermal gradient. The dashed lines demarcate zones where different creep mechanisms define the model's ductile substrate structure (see text). The left column of plots shows the case of finite cohesion in a 'Byerlee's rule' for ice, while the right column is for the case of zero cohesion (Beeman et al., 1988). The top row of plots is for an ice grain size of 0.1 mm, the middle row for 1 mm, and the bottom row for 10 mm. A critical growth rate q_{max} of ~200 should be exceeded to explain the observed folds near Astypalaea Linea on Europa.

The 25-km-wavelength contour indicates the combinations of shortening rate and thermal gradient that might explain the folds at Astypalaea. These plots demonstrate a growth rate of 200 that can be plausibly generated for λ=25 km. When the ice grain size is 1 mm or greater, q_{max} of 200 is achieved at high shortening rates ($>10^{-14}$ s^{-1}) and high thermal gradients ($>$20 K km^{-1}). For smaller grain sizes, the lower limits on shortening rate and thermal gradient drop (Fig. 3, top row),

but further progressive decreases in ice grain size below 0.1 mm do not result in further broadening of the acceptable parameter space, because at smaller grain sizes, grain-size-insensitive easy-slip controls the rate of flow. Higher surface temperatures produce weaker instabilities (smaller values of q_{max}) by increasing the *e*-folding depth of the substrate viscosity profile (see Dombard and McKinnon, 2001); for a surface temperature more appropriate to equatorial regions on Europa (110 K), a critical q_{max} of 200 cannot be achieved except for shortening rates $>10^{-13}$ s^{-1}, near the upper limit of what we consider plausible and then only for small grain sizes (Fig. 4).

The most important use of Fig. 3, besides demonstrating that sufficient amplification for viscous-plastic folding potentially exists on Europa, is in constraining the thermal gradient at the time of formation. For the range of larger ice grain sizes where the ductility of the ice is controlled by grain-size insensitive, power-law creep, we infer thermal gradients >20 K km^{-1}. Smaller grain sizes admit smaller thermal gradients. Below, we will argue that the compressional stresses required to drive folding on Europa are so large that non-synchronous rotation may be the only likely dominant stress source. If so, and because the slowest likely rotation rate is $\sim$10 Myr, we adopt 10^{-16} s^{-1} as our minimum likely shortening rate, which from the top panels in Fig. 3 implies thermal gradients >13 K km^{-1}. Due to the low resolution of Voyager images of Europa, the observational upper limit on the non-synchronous rotating rate from Hoppa et al. (1999) is not very restrictive, and Hoppa et al. (2001) presented an argument from overlapping cycloid ridge formation (in the Astypalaea Region no less) that Europa is actually non-synchronously rotating with a 250 kyr period (consistent with shortening rates $\sim 10^{-14}$ s^{-1}). Whether or not the latter is true, we adopt 10^{-13} s^{-1} as our maximum likely shortening rate, which, from the other panels in Fig. 3, implies thermal gradients <23 K km^{-1}.

Fig. 5 is similar to Fig. 3, but with contours of dominant wavelength to lithospheric thickness ratio, λ/H, plotted as a function of shortening rate and thermal gradient. For $q_{max}>200$ and our adopted range of shortening rates, 10^{-16}–10^{-13} s^{-1}, this ratio is constrained between 8.9 and 10. A λ/H of $\sim$10 appears to be one of the more robust results of this model, implying a lithosphere thickness, or depth to the BDT, of $\sim$2.5–2.8 km. This value in turn implies an overburden stress σ_{zz} on Europa of $\sim$3.1–3.5 MPa, and based on Eqs. (1a) and (1b), a horizontal compressional tectonic stress $\sigma_{xx}-\sigma_{zz}$ of $\sim$9–10 MPa (e.g. Fig. 2).

The tectonics of Europa's icy shell are often discussed in terms of various tidal components or effects, such as diurnal (daily) stresses, non-synchronous rotation, and polar wander (e.g. Greeley et al., 2004). Of these, only non-synchronous rotation can provide stresses approaching 10 MPa. Maximum compressive stresses reach 8.1 MPa in places on the equator for non-synchronous rotation, but this requires a full 90° of rotation of a coherent, elastic ice shell (Leith and McKinnon, 1996; Greeley et al., 2004). Towards the poles, the maximum compression is only two-thirds as great, however (Leith and McKinnon, 1996), making compressional folding by non-synchronous rotation stresses at Astypalaea problematical. Furthermore, the stress regime at high northern and southern latitudes is not uniformly compressional, but a combination of horizontal compression and orthogonal tension, implying shear or strike-slip as the preferred failure mode.

Prockter and Pappalardo (2000) argued that folds at Astypalaea Linea formed at the proper azimuth for non-synchronous rotation stresses, followed by subsequent rotation of the shell. So if the structures are indeed folds, then our analysis implies that additional compressional stresses must have acted in concert with those due to non-synchronous rotation, or that the model itself is incomplete or inadequate. Additional stress sources might be solid-state convection in the

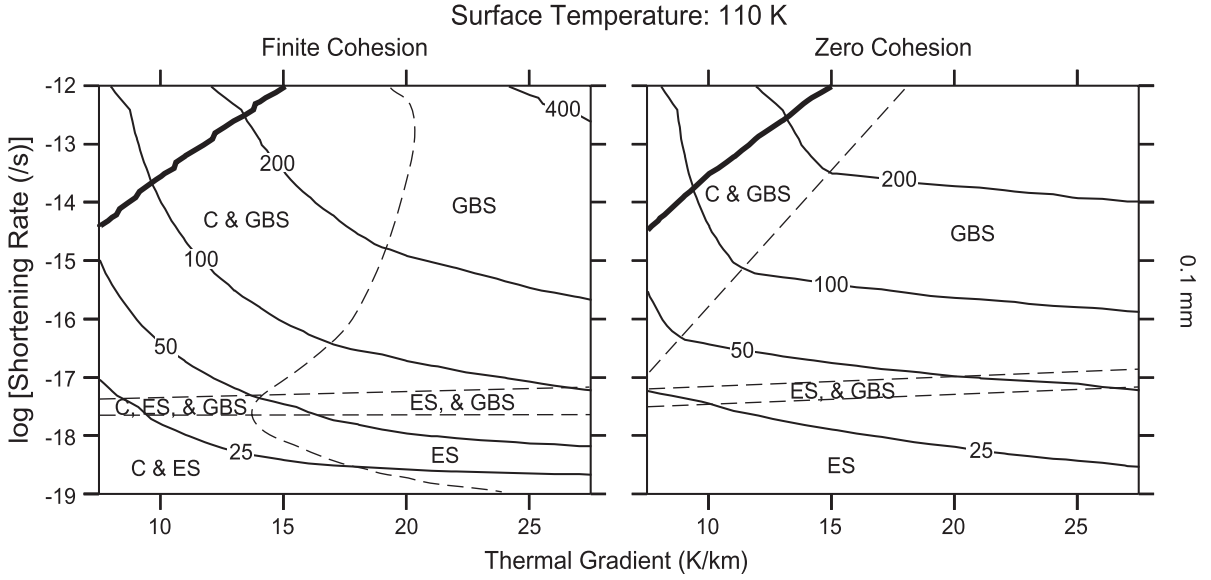

Fig. 4. Similar to Fig. 3, except assuming a surface temperature more appropriate to equatorial regions on Europa (110 K) and only showing the 'best' (maximally unstable) case of a grain size of 0.1 mm. While requirements of high thermal gradient and, hence, heat flow are relaxed, a sufficiently strong instability of the proper wavelength is only generated at very high rates of shortening.

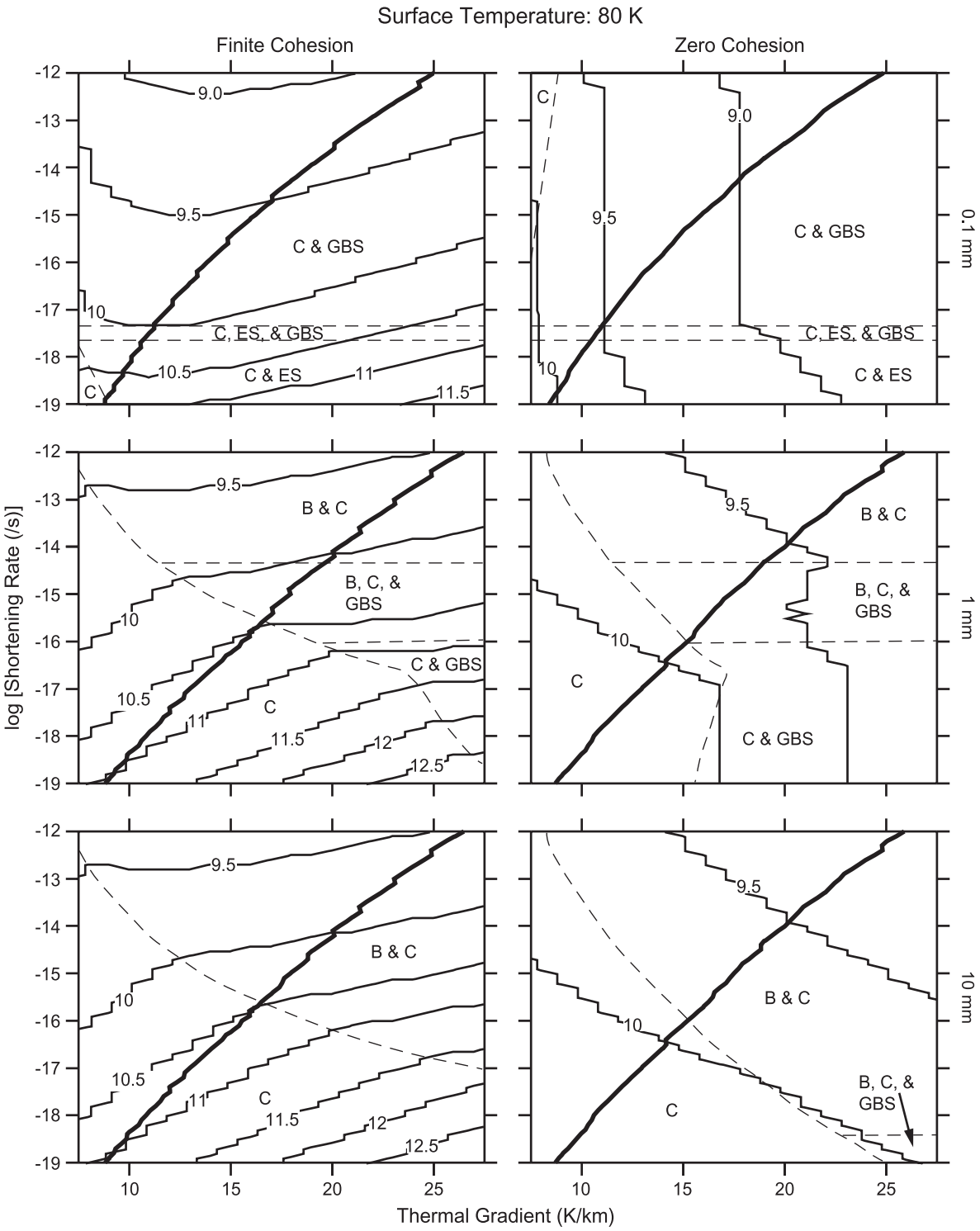

Fig. 5. Similar to Fig. 3, except showing contours of the wavelength to thickness ratio λ/H, instead of contours of q_{max} (the lack of smoothness in the contours is a numerical artifact). For $q_{max}>200$ and over the range of shortening rates considered plausible here (10^{-16}–10^{-13} s^{-1}), this ratio ranges between ~8.9 and 10 for instabilities 25 km in wavelength.

lower part of the shell (McKinnon, 1999; Solomatov, 2004) or compression from thermoelastic stresses and shell thickness changes due to a global or regional change in tidal heating (Nimmo, 2004). For example, a floating ice shell heating and thinning at its base would sink isostatically. Regardless, Nimmo (2004) developed his model in the context of a cooling shell to explain the predominantly *extensional* nature of Europa's surface. There is as yet no particular evidence for global or regional compression. As for the folding model, one possibility is that the shape of the strength envelope is not sharp as in Fig. 2, but blunted due to 'semi-brittle' deformation (Kohlstedt et al., 1995). Although there is

no concrete laboratory evidence for a semi-brittle regime in water ice, it is not implausible and could serve to lower the magnitude of the compressional stress needed to saturate the yield strength envelope, a condition that is required for this instability model.

Overall, however, our analysis illustrates the difficulty in explaining the folds at Astypalaea Linea in terms of viscous-plastic buckling. It is worth noting again that we assume plane-strain deformation; instabilities in non-plane-strain systems (e.g. transpression) may be reduced (Fletcher, 1995), making our predicted growth rates maximal in this respect. At the minimum, we suggest that the requirements for low surface temperature and high compressional stress are not commonly met on Europa, and that lithospheric folding is a relatively rare phenomenon. We note that relaxing our conservative criterion of a minimum growth rate of 200 has modest impact on our conclusions, because our assessment of required stresses and thermal structure is more limited by the minimum plausible shortening rate. A lower q_{max} (arguably less likely) does relax the restriction on grain size and allows for folding at more plausible shortening rates in equatorial regions; a higher q_{max} exacerbates the difficulty in generating folds by maintaining the grain size restriction and limiting the range of thermal gradients and stresses to the higher values.

Accepting the buckling model for Astypalaea Linea, we can convert the linear thermal gradients derived above into heat flows at this location. Because the thermal conductivity of ice is inversely proportional to temperature (Klinger, 1980), the thermal structure in the conductive portion of the icy shell of Europa (which covers the depths of interest here) is not linear with depth:

$$T = T_s \exp\left[\frac{Qz}{567}\right] \quad (5)$$

where T_s is surface temperature, Q is heat flow, and z is depth. What is critical to our model, however, is the temperature at the BDT. For a lithosphere thickness of 2.5–2.8 km, and a thermal gradient of 18 ± 5 K km^{-1}, this temperature is $\sim$112–144 K. The corresponding heat flow across the lithosphere is $\sim$75–125 mW m^{-2}. Thus, we conclude that $\sim$100 mW m^{-2} is an appropriate estimate of the heat flow during folding of Europa's icy lithosphere.

3. Topographic relaxation

3.1. Finite element simulations

The second stage of the evolutionary scenario proposed by Prockter and Pappalardo (2000) invoked rapid topographic relaxation; they estimated a relaxation time scale of $<10^5$ yr, assuming a constant, low viscosity of 10^{21} Pa s. The viscosity of Europan ice, however, should vary by many orders of magnitude over the greater than 170 K temperature range in the shell. Thus, we more thoroughly investigate this process here, using techniques detailed in Dombard and McKinnon (2000, 2006). We employ the commercially available MSC.MARC finite element package (http://www.mscsoftware.com), which permits concurrent simulation of elasticity, viscosity, and plasticity. These three behaviors capture the general behavior of geologic materials: solid on short time scales and fluid on long time scales, with brittle failure for large enough stress. To improve numerical stability, we do not include plasticity here; however, plasticity does not greatly affect the long-term relaxation of topography, and any effect is only manifested at large degrees of relaxation (Dombard and McKinnon, 2006).

3.1.1. Mesh and boundary conditions

Sinusoidal folds possess a natural symmetry; thus we implement a planar simulation of one half-wavelength, 12.5 km wide, evenly subdivided into 20 columns of elements. In the vertical direction, we consider the case of a thermal conductive ice shell 6.96 km deep, from Eq. (5), the depth at which the zero-pressure melting point of water is reached for T_s=80 K and Q=100 mW m^{-2}; this direction is subdivided into 25 elements biased to concentrate elements at the surface yet maintain element aspect ratios below $\sim$4. On the surface, we simulate sinusoidal topography with a 500 m crest-to-trough elevation difference, an overestimate of the topographic amplitude but one that should provide an upper bound on any original topography. On the base of the shell, the mesh is initially flat. The simulated space possesses a density of 950 kg m^{-3}.

Horizontal displacements on the side boundaries are locked, yielding a free-slip symmetry condition under the fold crest and trough. On the bottom boundary, we apply a foundational boundary condition that simulates the buoyant response of the liquid water ocean beneath the ice shell. In practice, this foundational force scales with displacement of the mesh boundary, with a scaling coefficient equal to the product of the gravitational acceleration (1.31 m s^{-2}) and the density of liquid water (assumed to be 1000 kg m^{-3}). The force of gravity is simulated via a gravitational body force uniformly applied to the entire mesh and equal to an acceleration of 1.31 m s^{-2}. Gravity supplies the stresses that drive relaxation; these driving stresses decay as the topography relaxes.

3.1.2. Material properties

The elastic parameters for ice are known: a Young's modulus of 9.3(3) GPa and a Poisson's ratio of 0.32(5) (Gammon et al., 1983). Simulation of such a compressible material subjected to a gravitational load would result in the generation of self-compaction deviatoric stresses, which can be compensated by adjusting the initial stress state (Dombard and McKinnon, 2000, 2006) to that of near-lithostatic equilibrium modulated solely by topographic driving stresses (see, e.g. Jaeger and Cook, 1979, p. 373). We bypass this step by letting Poisson's ratio approach 0.5 (0.4999), making the material nearly incompressible and thus eliminating the self-compaction. This step does modestly change the elastic response of the material; however, the primary elastic response under relaxation at finite heat flow is the development of an elastic

flexural layer (Dombard and McKinnon, 2006). Consequently, we compensate the larger Poisson's ratio by reducing the Young's modulus to 7.83 GPa, thereby maintaining the flexural rigidity of the icy layer (Eq. 3-72 in Turcotte and Schubert, 2002). As it is the viscosity structure that most strongly controls rates of relaxation (Dombard and McKinnon, 2006), any variations introduced by this incompressibility approximation are negligible.

The same ductile rheological parameters are used in our relaxation simulations as in our instability modeling; however, our numerical technique can implicitly handle the complexities introduced by the five interacting flow laws without the need for averaging schemes. The total strain rate is simply calculated at each point within the finite element mesh as a function of the stress and thermal state. We assume an ice grain size of 0.1 mm, to *maximize* creep. Time stepping is accomplished by an algorithm that maximizes time steps while restricting the change in creep strain relative to the elastic strain and the change in stress relative to the stress within prescribed tolerances. To keep the time steps from becoming too small to complete the simulations within a reasonable amount of computer time (hours to days), we limit the viscosity (proportional to the ratio of the deviatoric stress to total creep strain rate) in the mesh to be no less than a minimum value (generally between 10^{19} and 10^{22} Pa s, and much less than the viscosity of the cold surface).

3.1.3. Thermal structure

The presence of topography results in vertical deflection of the isotherms. To determine a realistic thermal state, we first perform a steady state simulation of thermal conduction, using the same mesh and the MSC.MARC finite element package, and then supplying the results to the relaxation simulations. Using the temperature-dependent thermal conductivity of ice (Klinger, 1980), we constrain the surface temperature to 80 K, inhibit heat flow through the side boundaries, and apply a heat flow of 100 mW m^{-2} to the base of the shell. Such heat flows may not be maintained indefinitely; in this regard, our results can be viewed as upper limit relaxation rates.

Two other cases also are considered. In the first, we maintain a surface temperature of 80 K but apply a heat flow of 150 mW m^{-2} (a generous upper limit allowed by our instability modeling). In the second, we apply a surface temperature of 110 K (appropriate to equatorial regions) and a heat flow of 75 mW m^{-2} (by Fig. 4, the higher surface temperature relaxes the requirement for high heat flow, but shortening rates are implausibly high). We do not change the thickness of the simulated space; thus for both these additional cases, these systems *in conductive steady state* would reach ice melting above the bottom of our mesh. We could envision a transition at depth to a more-or-less isothermal convective layer. The temperature in this layer would be about 10 K less than melting (McKinnon, 1999), and its relatively low viscosity is covered by our minimum viscosity limit. In addition, we will argue that our results are insensitive to the details in the deep mesh.

3.2. Results

Fig. 6 shows the evolution of the crest-to-trough elevation difference out to 100 Myr, a time likely greater than the mean surface age of Europa (Zahnle et al., 2003; Schenk et al., 2004). In the nominal case (T_s=80 K and Q=100 mW m^{-2}), the fold only relaxes by ~20 m over this time span. The reason for this retention is the relatively cool temperatures in the upper shell; for a heat flow of 100 mW m^{-2} and particularly a surface temperature of 80 K, the upper ~2.75 km of the shell is at temperatures of 130 K or less. Ice at these temperatures will not flow appreciably over even long geologic time scales, and viscous relaxation will be minor (essentially, an *elastic lithosphere* develops). A similar result was observed for relaxing craters at high latitudes (comparably low surface temperatures) on Ganymede and Callisto (Dombard and McKinnon, 2006).

The surface elastic lithosphere that develops over time flexes somewhat. For example, a 2.5–3-km-thick ice lithosphere loaded by harmonic topography of 250 m amplitude and λ=25 km should see the fold troughs and crests rise and subside, respectively, by ~5 m (Eq. 3-111 in Turcotte and Schubert, 2002). Consequently, a portion of the observed 20 m relaxation in Fig. 6 is due to this flexure, with relatively minor progressive creep in the flexing layer over long time scales. The flexural layer/elastic lithosphere is strong relative

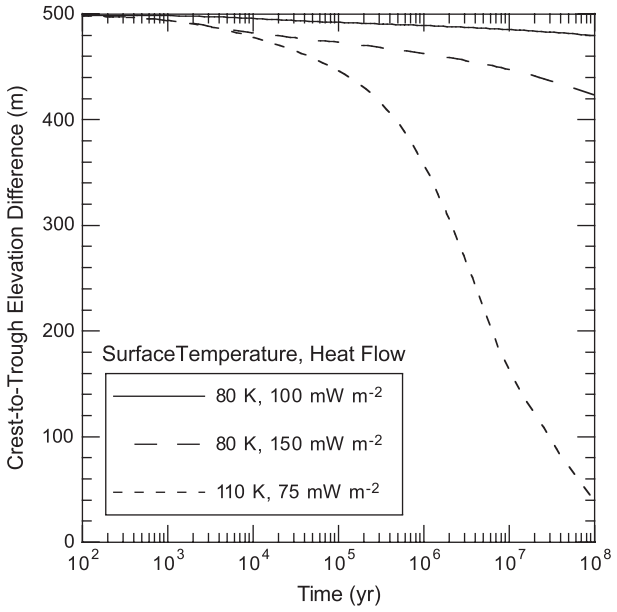

Fig. 6. Results of viscoelastic, finite element relaxation simulations, showing the crest-to-trough elevation difference as a function of time. Note that 500 m is twice the stereo-estimated present value at Astypalaea Linea. Combinations of surface temperature and heat flow are illustrated; the ice grain size in all cases is 0.1 mm, maximizing relaxation. While relaxation is an inefficient means to erase folds (i.e. decrease their topography to unobservable levels) at latitudes comparable with Astypalaea Linea, this mechanism could conceivably erase folds in equatorial regions over the lifetime of Europa's surface.

to the ductile substrate and serves to mechanically decouple the surface from the deeper shell. Thus, our results are insensitive to the details in the deep mesh (see also Dombard and McKinnon, 2006) and are also insensitive to the presence of basal topography or a thicker shell (surface heat flow can be maintained if the lower shell is convecting). We have run simulations of such test cases and find they are virtually indistinguishable from those shown in Fig. 6. A further consequence is that the simulated shell does not develop a 'keel' beneath the fold crest that isostatically supports the topography, which is instead supported by material strength in the near-surface layer.

A complementary case with T_s=80 K but Q=150 mW m^{-2} does exhibit greater relaxation, though not nearly enough to decrease the fold's topography to an unobservable level over 100 Myr (Fig. 6). Again, this retention is a consequence of the low surface temperature and strongly indicates that relaxation is an inefficient means of eliminating folds formed at higher latitudes. Conversely, relaxation may substantially reduce topographic amplitudes in equatorial regions in 10–100 Myr, even under lower heat flows (Fig. 6), because of the shallow depths of isotherms at which there can be appreciable creep over these time scales. On the other hand, our instability modeling suggests that lithospheric buckling at low latitudes is unlikely.

Because larger stresses result in faster flow in a non-Newtonian material, the compressional stresses in the icy shell from the folding process could conceivably affect the relaxation of topography. Schmeling (1987) has demonstrated that the interaction of two flow fields in a non-Newtonian fluid (here, flow associated with relaxation of topography and with relaxation of the remnant folding stresses) may result in either higher or lower viscosities, depending on the respective orientations of the flow fields (i.e. aligned, orthogonal, or against). To examine this effect, we perform simulations that are pre-stressed by displacing in the far boundary by 12 m, which generates compressive differential stresses of ~10 MPa and adds to the topography induced stresses. These simulations indicate that the relaxation of the folds proceeds at roughly the same rate, sometimes quicker and sometimes slower, than the cases without the pre-stress. Variances in the crest-to-trough elevation differences are less than ~20 m; remnant folding stresses thus do not affect subsequent relaxation significantly.

Greater relaxation on shorter time scales requires greater heat flows, especially towards the poles. Such elevated heat flows (>200 mW m^{-2}) are not impossible for Europa, but because they are not indicated by the buckling model, they are, at minimum, ad hoc. In particular, however, all of our simulations, despite some sensitivity to the imposed minimum viscosity limit, show only minor relaxation over the first 10^5 yr, the relaxation period proposed by Prockter and Pappalardo (2000). Indeed, after 10 Myr, all of our relaxation simulations possess observable, or at least geologically substantial, levels of retained topography, while many simulations show nearly pristine topography at times well in excess of the likely age of the surface. Thus, viscous relaxation does not appear to be a viable process to erase the folds such as these on Europa.

4. Discussion and conclusions

Our results suggest that the conditions under which the lithosphere of Europa may become unstable with respect to buckling may be rare. Low surface temperatures, high heat flow, and relatively high shortening rates, for ice grain sizes >1 mm, are simultaneously required. The situation is only exacerbated when required stress levels are considered. A prerequisite of the instability model is that the yield strength envelope be saturated in compression. For the brittle–ductile transitions indicated by the instability model, this requirement necessitates ~9–10 MPa of compression; purely elastic buckling requires even greater stresses, >25 MPa (Prockter and Pappalardo, 2000). Generating such large stresses on Europa is difficult. Diurnal eccentricity stresses are only of order 0.1 MPa (Greeley et al., 2004). Stresses due to 90° of non-synchronous rotation are of order 10 MPa (Leith and McKinnon, 1996) and therefore may be of sufficient magnitude; however, zones of coherent compression in a non-synchronously rotating shell are spatially limited and centered near the equator (Helfenstein and Parmentier, 1985), where the relatively high surface temperature produces a weak instability. As discussed earlier, it may be just possible to co-add enough compressive stress at high latitude, or semi-brittle plastic failure may reduce the horizontal compression necessary to saturate the yield stress envelope. The other requirements for the generation of a sufficiently strong instability, however, still need to be met.

There have only been a small number of possible folds identified on Europa (Figueredo and Greeley, 2000; Prockter and Pappalardo, 2000; Prockter et al., 2002). It is conceivable that this small number is due to observational biases (lack of suitable image coverage, the general unevenness of Europa's surface, etc.); however, we conclude that given the paucity of identified folds, the strict requirements for the generation of a compressional instability, and the inefficiency of topographic relaxation, folding of the lithosphere is a rare occurrence. If true, this conclusion suggests that folding is a rather minor mechanism on Europa, and the prodigious extension observed on the surface is likely compensated by some other means.

Acknowledgements

Sincere thanks to Ray Fletcher and Adam Showman for their reviews. AJD was partially funded by NASA Grant NAG5-13243 to Roger Phillips; we also thank him for use of his computational resources. The last push to publication was supported in part by indirect funds from The Johns Hopkins University Applied Physics Laboratory. This research was supported by NASA Planetary Geology and Geophysics grants NAG5-3657 and NAG5-11517 and Jupiter Systems Data Analysis Program grant NAG5-8899 to WBM.

References

Beeman, M., Durham, W.B., Kirby, S.H., 1988. Friction of ice. Journal of Geophysical Research 93, 7625–7633.

Brace, W.F., Kohlstedt, D.L., 1980. Limits on lithospheric stress imposed by laboratory experiments. Journal of Geophysical Research 85, 6248–6252.

De La Chappelle, S., Castelnau, O., Lipenkov, V., Duval, P., 1998. Dynamic recrystallization and texture development in ice as revealed by the study of deep ice cores in Antarctica and Greenland. Journal of Geophysical Research 103, 5091–5105.

Dombard, A.J., McKinnon, W.B., 2000. Long-term retention of impact crater topography on Ganymede. Geophysical Research Letters 27, 3663–3666.

Dombard, A.J., McKinnon, W.B., 2001. Formation of grooved terrain on Ganymede: extensional instability mediated by cold, superplastic creep. Icarus 154, 321–336.

Dombard, A.J., McKinnon, W.B., 2006. Elastoviscoplastic relaxation of impact crater topography, with application to Ganymede and Callisto. Journal of Geophysical Research doi:10.1029/2005JE002445.

Durham, W.B., Stern, L.A., 2001. Rheological properties of water ice—applications to satellites of the outer planets. Annual Reviews of Earth and Planetary Sciences 29, 295–330.

Figueredo, P.H., Greeley, R., 2000. Geologic mapping of the northern leading hemisphere of Europa from Galileo solid-state imaging data. Journal of Geophysical Research 105, 22629–22646.

Fink, J.H., Fletcher, R.C., 1981. In: Variations in Thickness of Ganymede's Lithosphere Determined by Spacings of Lineations. Abstracts of the Lunar and Planetary Conference XII, pp. 277–278.

Fletcher, R.C., 1995. Three-dimensional folding and necking of a power-law layer: are folds cylindrical, and, if so, do we understand why? Tectonophysics 247, 65–83.

Fletcher, R.C., Hallet, B., 1983. Unstable extension of the lithosphere: a mechanical model for basin-and-range structure. Journal of Geophysical Research 88, 7457–7466.

Fletcher, R.C., Hallet, B., 2004. Initiation of gneiss domes by necking, density instability, and erosion. In: Whitney, D.L., Teyssier, C., Siddoway, C.S. (Eds.), Gneiss Domes in Orogeny. Geological Society of America Special Paper 380, pp. 79–95.

Gammon, P.H., Kiefte, H., Clouter, M.J., 1983. Elastic constants of ice samples by Brillouin Spectroscopy. Journal of Physical Chemistry 87, 4025–4029.

Goldsby, D.L., Kohlstedt, D.L., 2001. Superplastic deformation of ice: experimental observations. Journal of Geophysical Research 106, 11017–11030.

Greeley, R., Chyba, C.F., Head, J.W., McCord, T.B., McKinnon, W.B., Pappalardo, R.T., Figueredo, P.H., 2004. Geology of Europa. In: Bagenal, F., Dowling, T.E., McKinnon, W.B. (Eds.), Jupiter: The Planet, Satellites, and Magnetosphere. Cambridge University Press, Cambridge, pp. 329–362.

Helfenstein, P., Parmentier, E.M., 1985. Patterns of fracture and tidal stresses due to nonsynchronous rotation: implications for fracturing on Europa. Icarus 61, 175–184.

Herrick, D.L., Stevenson, D.J., 1990. Extensional and compressional instabilities in icy satellite lithospheres. Icarus 85, 191–204.

Hoppa, G.V., Greenberg, R., Geissler, P., Tufts, B.R., Plassmann, J., Durda, D.D., 1999. Rotation of Europa: constraints from terminator and limb positions. Icarus 137, 341–347.

Hoppa, G.V., Tufts, B.R., Greenberg, R., Hurford, T.A., O'Brien, D.P., Geissler, P., 2001. Europa's rate of rotation derived from the tectonic sequence in the Astypalaea Region. Icarus 153, 208–213.

Jaeger, J.C., Cook, N.G.W., 1979. Fundamentals of Rock Mechanics. Chapman & Hall, London.

Klinger, J., 1980. Influence of a phase transition of ice on the heat and mass balance of comets. Science 209, 271–272.

Kohlstedt, D.L., Evans, B., Mackwell, S.J., 1995. Strength of the lithosphere: constraints imposed by laboratory experiments. Journal of Geophysical Research 100, 17587–17602.

Leith, A.C., McKinnon, W.B., 1996. Is there evidence for polar wander on Europa? Icarus 120, 387–398.

McKinnon, W.B., 1999. Convective instability in Europa's floating ice shell. Geophysical Research Letters 26, 951–954.

Nimmo, F., 2004. Stresses generated in cooling viscoelastic ice shells: application to Europa. Journal of Geophysical Research 109 (E12), E12001, doi:10.1029/2004JE002347.

Ojakangas, G.W., Stevenson, D.J., 1989. Thermal state of an ice shell on Europa. Icarus 81, 220–241.

Pappalardo, R.T., Belton, M.J.S., Breneman, H.H., Carr, M.H., Chapman, C.R., Collins, G.C., Denk, T., Fagents, S., Geissler, P.E., Giese, B., Greeley, R., Greenberg, R., Head, J.W., Helfenstein, P., Hoppa, G., Kadel, S.D., Klaasen, K.D., Klemaszewski, J.E., Magee, K., McEwen, A.S., Moore, J.M., Moore, W.B., Neukum, G., Phillips, C.B., Prockter, L.M., Schubert, G., Senske, D.A., Sullivan, R.J., Tufts, B.R., Turtle, E.P., Wagner, R., Williams, K.K., 1999. Does Europa have a subsurface ocean? Evaluation of the geological evidence. Journal of Geophysical Research 104, 24015–24056.

Pffifner, O.A., Ramsay, J.G., 1982. Constraints on geological strain rates: arguments from finite strain states of naturally deformed rocks. Journal of Geophysical Research 87, 311–321.

Prockter, L.M., Pappalardo, R.T., 2000. Folds on Europa: implications for crustal cycling and accommodation of extension. Science 289, 941–943.

Prockter, L.M., Head, J.W., Pappalardo, R.T., Sullivan, R.J., Clifton, A.E., Giese, B., Wagner, R., Neukum, G., 2002. Morphology of Europan bands at high resolution: a mid-ocean ridge-type rift mechanism. Journal of Geophysical Research 107 (E5), 5028, doi:10.1029/2000JE001458.

Sarid, A.R., Greenberg, R., Hoppa, G.V., Hurford, T.A., Tufts, B.R., Geissler, P., 2002. Polar wander and surface convergence of Europa's ice shell: evidence from a survey of strike-slip displacement. Icarus 158, 24–41.

Schenk, P.M., 2002. Thickness constraints on the icy shells of the Galilean satellites from a comparison of crater shapes. Nature 417, 419–421.

Schenk, P.M., 2005. In: The Crop Circles of Europa. Abstracts of the Lunar and Planetary Conference XXXIII, p. 2081.

Schenk, P.M., Chapman, C.R., Zahnle, K., Moore, J.M., 2004. Ages and interiors: the cratering record of the Galilean satellites. In: Bagenal, F., Dowling, T.E., McKinnon, W.B. (Eds.), Jupiter: The Planet, Satellites, and Magnetosphere. Cambridge University Press, Cambridge, pp. 427–456.

Schmeling, H., 1987. On the interaction between small- and large-scale convection and postglacial rebound flow in a power-law mantle. Earth and Planetary Science Letters 84, 254–262.

Solomatov, V.S., 2004. Initiation of subduction by small-scale convection. Journal of Geophysical Research 109 (B1), B01412, doi:10.1029/2003JB002628.

Souchez, R.A., Lorrain, R.D., 1991. Ice Composition and Glacier Dynamics. Springer-Verlag, Berlin.

Turcotte, D.L., Schubert, G., 2002. Geodynamics, 2nd ed. Cambridge University Press, New York.

Zahnle, K., Schenk, P., Levison, H., Dones, L., 2003. Cratering rates in the outer solar system. Icarus 163, 263–289.

Zuber, M.T., 1987. Compression of oceanic lithosphere: an analysis of intraplate deformation in the Central Indian Basin. Journal of Geophysical Research 92, 4817–4825.

Zuber, M.T., Parmentier, E.M., 1996. Finite amplitude folding of a continuously viscosity-stratified lithosphere. Journal of Geophysical Research 101, 5489–5498.